Precipitation synthesis and magnetic properties of self-assembled magnetite-chitosan nanostructures

Oleksii Bezdorozhev, Taras Kolodiazhnyi, Oleg Vasylkiv*

National Institute for Materials Science

1–2–1, Sengen, Tsukuba, Ibaraki 305–0047, Japan

*Corresponding Author

Vasylkiv O.: e-mail: oleg.vasylkiv@nims.go.jp, phone: +81-(0)80-4144-4747

Abstract

This paper reports the synthesis and magnetic properties of unique magnetite-chitosan nanostructures synthesized by the chemical precipitation of magnetite nanoparticles in the presence of chitosan. The influence of varying synthesis parameters on the morphology of the magnetic composites is determined. Depending on the synthesis parameters, magnetite-chitosan nanostructures of spherical (9–18 nm), rice-seed-like (75–290 nm) and lumpy (75–150 nm) shapes were obtained via self-assembly. Spherical nanostructures encapsulated by a 9–15 nm chitosan layer were assembled as well. The prospective morphology of the nanostructures is combined with their excellent magnetic characteristics. It was found that magnetite-chitosan nanostructures are ferromagnetic and pseudo-single domain. Rice-seed-like nanostructures exhibited a coercivity of 140 Oe and saturation magnetization of 56.7 emu/g at 300 K. However, a drop in the magnetic properties was observed for chitosan-coated spherical nanostructures due to the higher volume fraction of chitosan.

Keywords: Chitosan; Magnetite; Magnetic properties; Nanostructures; Precipitation

1. Introduction

Iron oxide nanoparticles have been intensely studied in the last decades for their unique properties. Among the iron oxides, magnetite (Fe_3O_4) and maghemite (γ-Fe_2O_3), both of which possess similar face centered cubic close-packed structure, are of significant interest due to their magnetic and biological properties [1, 2]. Potential application of magnetite and maghemite nanoparticles include biomedicine, water treatment, catalysis, electronic devices, etc [1–3]. Some of the clinical applications include contrast agents for magnetic resonance imaging, targeted drug delivery, protein immobilization, hyperthermia agents for cancer treatment, embolotherapy, tissue repair, bioseparation, biosensors, and cell labeling [4, 5]. The very wide potential for the utilization of iron oxide nanoparticles is due to the combination of magnetic properties with biocompatibility, reactive surface, stability, and innocuousness. Much attention has been focused on the synthesis of iron oxide nanoparticles since a preparation method and parameters have a considerable effect on the properties of nanoparticles. The wet chemical methods for the synthesis of monodisperse nanoparticles have been well-established in the recent past. Chemical precipitation, thermolysis, sol-gel, microemulsion, hydrothermal, electrochemical syntheses are usually used to synthesize iron oxide and other nanoparticles [1, 2, 6–11]. Due to the enormous progress in this field, nanoparticles with controllable morphology, composition and crystallinity are available. Among the developed methods, biological synthesis or synthesis in the

presence of organic compounds in aqueous reaction mixtures is an attractive way not only to reduce the use or generation of hazardous substances, but also to control the nucleation, growth and agglomeration processes of various nanoparticles [12–14]. For this purpose, chitosan has been used as a key component for the synthesis of many functional materials [3, 5, 15, 16]. Chitosan is a linear aminopolysaccharide, which possesses biocompatibility, biodegradability, bioadhesion for many biomacromolecules and high tendency to form chelate complexes. Magnetite nanoparticles can be easily coated with chitosan and other species like dextran, polyethylene glycol, silica, and gold for tailoring of selected properties and surface functionalization [17]. Due to the presence of hydroxy and aminogroups [18], chitosan has been used as a surface modifier, reducing and stabilizing agent to control the size, shape, and aggregation of nanoparticles [3, 4, 16, 17, 19].

It is of fundamental and practical interest to organize magnetic nanoparticles into new multifunctional nanostructures with superior properties. Recently, it was confirmed that chitosan causes morphological, orientational, and growth mechanism changes in the crystals nucleation [20–26] and can be used as a morphology-directing agent for the preparation of petunia-shaped $CaCO_3$ superstructures [22], I-, Y-, T-, X-shaped Se/C nanorods [23], curved fiber-like Ni-Al-CO_3 hydroxides [24], spherical, tabular, and carambola-like silica particles [25].

In our previous study [26], we showed that due to the functional amino groups of chitosan the cubo-octahedral, flower-like, rod-like Fe_3O_4 nanoparticles change their morphology to cubic, quasi-spherical and rice-seed-like structures, respectively, when chitosan was added to the solutions at various synthesis parameters. In this paper, we build on our previous research [26] by studying the magnetic properties of magnetite-chitosan nanostructures as well as the effect of different synthesis parameters, such as

time, iron ions and chitosan concentrations, on the morphology of the nanostructures precipitated at 80 ^{o}C.

2. Materials and methods

2.1. Synthesis of magnetite-chitosan nanostructures

Magnetite-chitosan nanostructures were synthesized by the precipitation method using iron chloride precursors with the addition of chitosan and urea as a precipitating agent. The aqueous solutions were prepared by dissolving $FeCl_2 \cdot 4H_2O$ and $FeCl_3 \cdot 6H_2O$ (99%, Wako Pure Chemical Industries Ltd., Japan) in deionized water at concentrations of 0.01–0.08 M Fe^{2+} and 0.02–0.16 M Fe^{3+} in a 1:2 molar ratio. To this solution was added chitosan acetic solution, which was previously prepared by dissolving chitosan (400 kDa, 87% degree of deacetylation, Fluka BioChemika, Japan) in a 0.1 mol/l aqueous acetic acid solution. The weight ratio of chitosan to iron chlorides was 1:1 and 3:1. Then, urea (NH_2CONH_2, 99%, Kanto Chemical Co., Japan) was added into the solution at the weight ratio of iron chlorides to urea of 1:2 and stirred at room temperature for 10 h. The synthesis was carried out at 80 °C for 10–50 h using a magnetic stirrer with a hot plate in a nitrogen environment to promote the formation of pure Fe_3O_4 phase nanoparticles and prevent their oxidation.

The precipitate was washed twice with distilled water and absolute ethanol (99.5% reagent grade) by an ultrasonic and a centrifuge to remove anion impurities, break up powder agglomerates and to separate the powder from the supernatant. After drying at 80 ^{o}C, the solid was annealed at 350 ^{o}C in a N_2 atmosphere for 1 h to improve the crystallinity of the nanoparticles.

2.2. Characterization

Transmission electron microscopy (TEM) equipped with energy dispersive spectrometer (EDS) was employed to study the size and shape of the precipitated products by a JEM-2100-F microscope (JEOL Ltd., Japan) operated at 200 kV. The samples for TEM analysis were prepared by pipetting a droplet of the suspension on a Cu grid with a carbon coating and allowed to dry at room temperature. X-ray powder diffraction (XRD) measurements were performed on a Rigaku Ultima III diffractometer (Rigaku Corp., Japan) operated at 40 kV and 40 mA with Cu *Kα* radiation (λ = 1.5406 Å) in the 2θ range from 20–80 ^{o} with a scanning rate of 0.15 ^{o}/min and a step size of 0,01^{o}. The magnetic properties of the samples were measured at temperatures of 10 K and 300 K in the applied fields from –30 kOe to 30 kOe using a superconducting quantum interference device (SQUID) MPMS XL (Quantum Design, USA).

3. Results and discussion

3.1. Synthesis of magnetite-chitosan nanostructures

In order to investigate the effect of the concentration of iron ions on the size and morphology of magnetite-chitosan nanostructures, a series of experiments were carried out. The processing conditions and characteristics of the synthesized magnetite-chitosan nanostructures are summarized in Table 1. Fig. 1(a) shows the XRD pattern of nanostructures obtained by the precipitation at 80 ^{o}C for 50 h from the aqueous solution with 0.01 M $FeCl_2$ and 0.02 M $FeCl_3$ concentration, and weight ratio of chitosan to iron

chlorides of 1:1. The results of the XRD analysis showed that nanoparticles synthesized according to the reactions (1, 2) are single-phase Fe_3O_4 nanoparticles after annealing at 350 °C under a N_2 atmosphere.

$$(NH_2)_2CO + 3H_2O \rightarrow 2NH_4OH + CO_2\uparrow \quad (1)$$

$$FeCl_2 + 2FeCl_3 + 8NH_4OH \rightarrow Fe_3O_4 + 8NH_4Cl + 4H_2O \quad (2)$$

The diffraction peaks on Fig. 1(a) at $2\theta \approx 30{,}0^{o}$; 35,4 °; 37,0 °; 43,0 °; 53,4 °; 56,9 °; 62,5 °; 70,9 °; 73,9 °; 74,9 °; 78,9 ° correspond to magnetite with cubic spinel structure (DB card No. 9006242). The XRD peaks of chitosan were not detected in the investigated samples possibly due to its amorphous structure and/or degradation during annealing in N_2 at 350 °C [27].

In Fig. 1(b) is shown a TEM image of magnetite-chitosan nanostructures precipitated from aqueous solution with 0.01 M $FeCl_2$ and 0.02 M $FeCl_3$ concentration. The obtained nanostructures have a lumpy shape and formed from hard mesoporous aggregates, which, in turn, formed from the nanoparticles. The size of the nanostructures is 75–150 nm, while the size of the round-shaped aggregates varies in the range of 20–65 nm. Since the synthesis was carried out in the aqueous iron chloride solution with chitosan addition, it can be suggested that chitosan interacted with iron ions and hydroxyl groups on the surface of Fe_3O_4 by means of functional amino groups [3, 15–25], as schematically depicted in Fig. 2. As a result, the growth of the separate iron oxide nuclei is inhibited and the formed nuclei aggregate. Then, iron oxide nanocrystals slowly grow on the surface of these aggregates, which is followed by their self-assembly into polycrystalline nanostructures [20, 22, 24, 26]. The mesoporous structure of the synthesized materials supports the above statement that they are formed from several nanocrystals.

In Fig. 3(a) is presented the XRD pattern for the sample obtained by the precipitation from the solution with 0.05 M $FeCl_2$ and 0.1 M $FeCl_3$ concentration at 80 ^oC for 10 h. According to the XRD analysis, the selected synthesis parameters are responsible for the formation of a single phase product, namely magnetite with the diffraction peaks at $2\theta \approx 30{,}0^o$; 35,4 ^{o}; 37,0 ^{o}; 43,0 ^{o}; 53,4 ^{o}; 56,9 ^{o}; 62,5 ^{o}; 70,9 ^{o}; 73,9 ^{o}; 74,9 ^{o}; 78,9 ^{o}. All peaks are in good accordance with the standard spectrum for Fe_3O_4 (DB card No. 9006242). As expected, the same phase composition was found for rice-seed-like nanostructures, which were obtained after precipitation at 80 ^{o}C for 50 h [26].

The TEM image of the magnetite-chitosan nanostructures precipitated at 80 ^{o}C for 10 h is shown in Fig. 3(b). According to Fig. 3(b), magnetite nanoparticles are 9–18 nm in size and have a shape close to spherical one. To reduce surface energy the nanoparticles formed agglomerates with sizes up to 80 nm. According to [20–26], we suppose that due to the adsorption of chitosan molecules onto the surface of iron oxide crystals their growth rate is drastically reduced. As a result, nanocrystals form spherical nanostructures due to surface energy minimization.

The rice-seed-like nanostructures with the length and diameter of 75–290 nm and 70–145 nm, respectively, were obtained when the synthesis time was prolonged to 50 h (Fig. 4). The length to diameter ratio of the formed nanostructures was in the range of 1.1–2.5, indicating that their shape varies from almost spherical to ellipsoidal. The nanostructures with quasi-spherical shape and sizes ranged from 90 nm to 130 nm were also observed in insignificant quantity. As calculated from the TEM images, the quantity of the quasi-spherical nanostructures was about 20% of the total quantity for the selected synthesis parameters. Using EDS, chitosan was found in rice-seed-like nanostructures, according to the distribution maps of the Fe, O, C, N elements in Fig. 4, since the nitrogen and carbon atoms of chitosan with 87% degree of deacetylation were

detected. The elemental mapping demonstrates the uniform distribution of the elements indicating good homogeneity of the rice-seed-like nanostructures. The obtained results also suggest that the synthesis of magnetite nanoparticles in the presence of chitosan leads to the formation of magnetite-chitosan nanocomposites.

These nanostructures are formed through the self-assembly of the spherical nanoparticles into rice-seed-like or quasi-spherical nanostructures. According to [20, 22, 24, 26], the formation process of the magnetite-chitosan nanostructures occurs through the adsorption of biopolymer molecules on the surface of the nanocrystals, aggregation, slow crystal growth on the surface of these aggregates, and their self-assembly into polycrystalline structures.

An increase of iron chloride concentration to 0.08 M $FeCl_2$ and 0.16 M $FeCl_3$ leads to the precipitation of the rice-seed-like nanostructures (Fig. 5), which are similar to that obtained at lower iron ions concentration (0.05 M $FeCl_2$ and 0.1 M $FeCl_3$).

Fig. 6 shows a TEM image of the magnetite-chitosan nanostructures obtained from the solution with 0.05 M $FeCl_2$ and 0.1 M $FeCl_3$ concentration and the weight ratio of chitosan to iron chlorides of 3:1. From Fig. 6, it can be seen that the nanoparticles formed mesoporous nanostructures with nearly spherical shape. The size of the obtained nanostructures varied in the range of 35–120 nm, while their average size was 81±9 nm. Furthermore, the spherical nanostructures were coated with a layer of chitosan of 9–15 nm thickness, as shown in Fig. 6. The elemental mapping results in Fig. 7 confirm that those nanostructures consist of both magnetite and chitosan forming nanocomposite encapsulated with chitosan.

The formation of chitosan coated nanostructures is similar to that of rice-seed-like nanostructures. However, in this case, the concentration of chitosan in the solution was three times higher. Thus, we believe that the amount of the adsorbed chitosan

molecules onto magnetite nanocrystals in the early stages of the synthesis process is also significantly increased, which in turn promotes the formation of spherically shaped nanostructures instead of rice-seed-like one. The excess of chitosan then precipitates on the spherical nanostructures to form a coating.

3.2. Magnetic properties of magnetite-chitosan nanostructures

Magnetic characteristics were experimentally investigated for rice-seed-like and chitosan coated nanostructures at 10 K and 300 K in the applied magnetic field of ±30 kOe. The magnetization of the rice-seed-like nanostructures is shown in Fig. 8(a). As can be seen from the *M–H* plots and their enlargement near the origin (lower right inset), the coercivity (*Hc*) of the sample is 400 Oe and 140 Oe at 10 K and 300 K, respectively, indicating their ferrimagnetic behavior. The ferrimagnetism of magnetite is caused by antiparallel, but unequal magnetic moments of two interpenetrating sublattices of Fe_3O_4. This also indicates that the size of the rice-seed-like nanostructures is larger than the critical one for transition from ferrimagnetic to superparamagnetic state [1]. The lower value of H_C at 300 K is attributed to the thermal fluctuation of the magnetic moments that overcome the magnetic anisotropy and reduce the coercivity [28].

The rice-seed-like nanostructures possessed a saturation magnetization (*Ms*) of 56.7 emu/g and saturation remanence (*Mr*) of 10.7 emu/g at 300 K. The *Ms* and *Mr* values slightly increased to 60.6 emu/g and 20 emu/g at 10 K, respectively. This behavior is typical for magnetite and can be attributed to the decrease in thermal energy [29].

On the basis of *Mr*/*Ms* ratio or squareness (*Sr*) the magnetic structure of the samples can be determined. The *Sr* values were found to be 0.33 and 0.19 at 10 K and 300 K, respectively. According to [30, 31], it can be concluded that the rice-seed-like nanostructures are pseudo-single domain since the *Sr* values are in the range of 0.1–0.5. This suggests that the samples have an almost uniform magnetization. The self-assembly of the magnetite nanoparticles and chitosan into rice-seed-like nanostructures result in the change of the single domain to the pseudo-single domain magnetic structure, leading to nonzero coercivity.

Table 2 summarizes the properties of the various magnetite-chitosan composites obtained in our study and those reported in the other investigations [32–48]. The observed large divergence of the magnetic characteristics in the literature data is mainly attributed to different amount of chitosan in the composites. The obtained *Ms* values of the rice-seed-like nanostructures correspond to those found in the literature for magnetite-chitosan composites and imply the strong magnetic response to the magnetic field. However, the *Ms* values were found to be almost one-third lower than that for bulk magnetite (92 emu/g) [49] since the obtained nanostructures contain chitosan, which is a diamagnetic material [35]. The decrease of *Ms* is related to the amount of chitosan that quenches the surface moments of magnetic nanoparticles and decreases the volume fraction of the magnetic phase [27]. The reduction of the saturation magnetization also could be attributed to the surface spin canting and imperfection of the samples compared to the bulk Fe_3O_4.

Fig. 8(b) shows the magnetic hysteresis loops of chitosan coated nanostructures. The coercive field of 200 Oe was observed at 10 K, while the smaller one of 80 Oe was observed at 300 K, indicating that the nanostructures are in a ferrimagnetic state. According to the obtained *Mr* and *Ms* values, the samples were also found to be pseudo-

single domain, since *Sr* were in the range of 0.1–0.17. The *Ms* for chitosan coated nanostructures is 30 emu/g at 10 K and 27.2 emu/g at 300 K, which is typical for magnetite-chitosan composites as reported in the literature [27, 32–48]. It can be also observed from Fig. 8 that the saturation magnetization and coercivity of the samples significantly decreased in comparison with that of the rice-seed-like nanostructures. Since the magnetic properties originate from magnetic nanoparticles, it is clear that chitosan in the nanostructures and chitosan coating decreased the volume fraction of magnetite, resulting in deterioration of magnetic properties.

4. Conclusions

We investigated for the first time the magnetic characteristics and morphology of the magnetite-chitosan nanostructures prepared via chemical precipitation of magnetite nanoparticles by urea in the presence of chitosan at 80 ^{o}C. It was shown that spherical magnetite-chitosan nanostructures (9–18 nm) can be obtained at 80 ^{o}C for 10 h, while rice-seed-like nanostructures (75–290 nm) are formed when the synthesis time was increased to 50 h. Magnetite-chitosan nanostructures with lumpy shape also can be obtained at lower concentration of iron ions. When the synthesis was conducted at a threefold higher concentration of chitosan, the spherical nanostructures (35–120 nm) with 9–15 nm thick layer of chitosan were precipitated. It was found that rice-seed-like nanostructures and chitosan coated nanostructures are ferrimagnetic and pseudo-single domain. The coercivity and saturation magnetization of the rice-seed-like nanostructures at 300 K was found to be 140 Oe and 56.7 emu/g, respectively. While the coercivity of 80 Oe and saturation magnetization of 27.2 emu/g was measured for chitosan coated spherical nanostructures. An almost twofold higher coercivity and saturation

magnetization of rice-seed-like nanostructures was explained by lower volume fraction of chitosan in the former. The obtained magnetite-chitosan nanostructures can be used in various biomedical applications.

References

[1] D.L. Huber, Synthesis, properties, and applications of iron nanoparticles, Small. 1 (5) (2005) 482-501.

[2] S. Laurent, D. Forge, M. Port, A. Roch, C. Robic, L.V. Elst, R.N. Muller, Magnetic iron oxide nanoparticles: synthesis, stabilization, vectorization, physicochemical characterizations, and biological applications, Chem. Rev. 108 (6) (2008) 2064-2110.

[3] D.H.K. Reddy, S.-M. Lee, Application of magnetic chitosan composites for the removal of toxic metal and dyes from aqueous solutions, Adv. Colloid Interface Sci. 201-202 (2013) 68-93.

[4] A. Chandna, D. Batra, S. Kakar, R. Singh, A review on target drug delivery: magnetic microspheres, JAD 2 (3) (2013) 189-195.

[5] T. Neuberger, B. Schopf, H. Hofmann, M. Hofmann, B. von Rechenberg, Superparamagnetic nanoparticles for biomedical applications: possibilities and limitations of a new drug delivery system, J. Magn. Magn. Mater. 293 (1) (2005) 483-496.

[6] S.F. Hasany, N.H. Abdurahman, A.R. Sunari, R. Jose, Magnetic iron oxide nanoparticles: chemical synthesis and applications review, Curr. Nanosci. 9 (5) (2013) 561-575.

[7] M. Mohapatra, S. Anand, Synthesis and applications of nano-structured iron oxides/hydroxides – a review, Int. J. Eng. Sci. Technol. 2 (8) (2010) 127-146.

[8] F.N. Sayed, V. Polshettiwar, Facile and sustainable synthesis of shaped iron oxide nanoparticles: Effect of iron precursor salts on the shapes of iron oxides, Sci. Rep. 5 (2015) 1-14.

[9] O. Vasylkiv, Y. Sakka, Y. Maeda, V.V. Skorokhod, Nano-engineering of zirconia-noble metals composites, J. Eur. Ceram. Soc. 24 (2) (2004) 469-473.

[10] O. Vasylkiv, Y. Sakka, Y. Maeda, V.V. Skorokhod, Sonochemical preparation and properties of Pt-3Y-TZP nano-composites, J. Am. Ceram. Soc. 88 (3) (2005) 639-644.

[11] O. Vasylkiv, Y. Sakka, V.V. Skorokhod, Nano-blast synthesis of nanosize CeO_2-Gd_2O_3 powders, J. Am. Ceram. Soc. 89 (6) (2006) 1822-1826.

[12] L.C. Preiss, K. Landfester, R. Munoz-Espi, Biopolymer colloids for controlling and templating inorganic synthesis, Beilstein J. Nanotechnol. 5 (2014) 2129-2138.

[13] H. Colfen, S.-H. Yu, Biomimetic mineralization/synthesis of mesoscale order in hybrid inorganic-organic materials via nanoparticle self-assembly, MRS Bull. 30 (10) (2005) 727-735.

[14] S. Gao, Y. Shi, S. Zhang, K. Jiang, S. Yang, Z. Li, E. Takayama-Muromachi, Biopolymer-assisted green synthesis of iron oxide nanoparticles and their magnetic properties, J. Phys. Chem. 112 (28) (2008) 10398-10401.

[15] G.A. Kloster, N.E. Marcovich, M.A. Mosiewicki, Composite films based on chitosan and nanomagnetite, Eur. Polym. J. 66 (2015) 386-396.

[16] A. Kaushik, P.R. Solanki, A.A. Ansari, G. Sumana, S. Ahmad, B.D. Malhotra, Iron oxide-chitosan nanobiocomposite for urea sensor, Sens. Actuators, B 138 (2) (2009) 572-580.

[17] S. Bagheri, N.M. Julkapli, Modified iron oxide nanomaterials: functionalization and application, J. Magn. Magn. Mater. 416 (2016) 117-133.

[18] M. Rinaudo, Chitin and chitosan: properties and applications, Prog. Polym. Sci. 31 (7) (2006) 603-632.

[19] Y.-K. Twu, Y.-W. Chen, C.-M. Shih, Preparation of silver nanoparticles using chitosan suspensions, Powder Technol. 185 (3) (2008) 251-257.

[20] A.W. Ritchie, M.I.T. Watson, R. Turnbull, Z.Z. Lu, M. Telfer, J.E. Gano, K. Self, H.F. Greer, W. Zhou, Reversed crystal growth of rhombohedral calcite in the presence of chitosan and gum arabic, CrystEngComm. 15 (47) (2013) 10266-10271.

[21] K. Kim, A. Uysal, S. Kewalramani, B. Stripe, P. Dutta, Effects of chitosan on the alignment, morphology and shape of calcite crystals nucleating under Langmuir monolayers, CrystEngComm. 11 (1) (2009) 130-134.

[22] P. Liang, Q. Shen, Y. Zhao, Y. Zhou, H. Wei, I. Lieberwirth, Y. Huang, D. Wang, D. Xu, Petunia-shaped superstructures of $CaCO_3$ aggregates modulated by modified chitosan, Langmuir 20 (24) (2004) 10444-10448.

[23] B. Yu, T. Chen, F. Yang, W. Liu, Y.-H. Li, W. Zheng, Chitosan as morphology-directing agent for the preparation of multiarmed selenium/carbon coaxial nanorods, Chem. Lett. 40 (3) (2011) 242-243.

[24] B. Li, J. He, D.G. Evans, X. Duan, Morphology and size control of Ni–Al layered double hydroxides using chitosan as template, J. Phys. Chem. Solids. 67 (5-6) (2006) 1067-1070.

[25] B. Leng, X. Chen, Z. Shao, W. Ming, Biomimetic synthesis of silica with chitosan-mediated morphology, Small 4 (6) (2008) 755-758.

[26] O. Vasylkiv, O. Bezdorozhev, Y. Sakka, Synthesis of iron oxide nanoparticles with different morphologies by precipitation method with and without chitosan addition, J. Ceram. Soc. of Japan 124 (4) (2016) 489-494.

[27] G. Unsoy, S. Yalcin, R. Khodadust, G. Gunduz, U. Gunduz, Synthesis optimization and characterization of chitosan-coated iron oxide nanoparticles produced for biomedical applications, J. Nanopart. Res. 14 (11) (2012) 964-977.

[28] Y.-H. Son, J.-K. Lee, Y. Soong, D. Martello, M. Chyu, Enhanced magnetic response of fluids using self-assembled petal-like iron oxide particles, Appl. Phys. Lett. 96 (12) (2010) 121905.

[29] D.H. Chen, Y.Y. Chen, Synthesis of barium ferrite ultrafine particles by coprecipitation in the presence of polyacrylic acid, J. Colloid Interface Sci. 235 (1) (2001) 9-14.

[30] F.D. Stacey, The physical theory of rock magnetism, Adv. Phys. 12 (45) (1963) 45-133.

[31] D.J. Dunlop, Magnetite: behavior near the single-domain threshold, Science 176 (4030) (1972) 41-43.

[32] K. Donadel, M.D.V. Felisberto, V.T. Favere, Synthesis and characterization of the iron oxide magnetic particles coated with chitosan biopolymer, Mater. Sci. Eng., C 28 (4) (2008) 509-514.

[33] H.V. Tran, L.D. Tran, T.N. Nguyen, Preparation of chitosan/magnetite composite beads and their application for removal of Pb(II) and Ni(II) from aqueous solution, Mater. Sci. Eng., C. 30 (2) (2010) 304-310.

[34] D.H. Kim, K.N. Kim, K.M. Kim, Y.K. Lee, Targeting to carcinoma cells with chitosan- and starch-coated magnetic nanoparticles for magnetic hyperthermia, J. Biomed. Mater. Res. Part A 88 (1) (2009) 1-11.

[35] S. Zhang, Y.F. Zhou, W.Y. Nie, L.Y. Song, Preparation of Fe_3O_4/chitosan/poly(acrylic acid) composite particles and its application in adsorbing copper ion (II), Cellulose 19 (6) (2012) 2081-2091.

[36] K.M. Gregorio-Jauregui, Ma.G. Pineda, J.E. Rivera-Salinas, G. Hurtado, H. Saade, J.L. Martinez, A. Ilyina, R.G. Lopez, One-step method for preparation of magnetic nanoparticles coated with chitosan, J. Nanomater. 2012 (2012) 1-8.

[37] M. Shen, Y. Yu, G. Fan, G. Chen, Y.M. Jin, W. Tang, W. Jia, The synthesis and characterization of monodispersed chitosan-coated Fe_3O_4 nanoparticles via a facile one-step solvothermal process for adsorption of bovine serum albumin, Nanoscale Res. Lett. 9 (1) (2014) 296-303.

[38] W. Jiang, W. Wang, B. Pan, Q. Zhang, W. Zhang, L. Lv, Facile fabrication of magnetic chitosan beads of fast kinetics and high capacity for copper removal, ACS Appl. Mater. Interfaces 6 (5) (2014) 3421-3426.

[39] R.G. Lopez, M.G. Pineda, G. Hurtado, Chitosan-coated magnetic nanoparticles prepared in one step by reverse microemulsion precipitation, Int. J. Mol. Sci. 14 (10) (2013) 19636-19650.

[40] D. Dorniani, M.Z.B. Hussein, A.U. Kura, S. Fakurazi, A.H. Shaari, Z. Ahmad, Sustained release of prindopril erbumine from its chitosan-coated magnetic nanoparticles for biomedical applications, Int. J. Mol. Sci. 14 (10) (2013) 23639-23653.

[41] P.B. Shete, R.M. Patil, N.D. Thorat, A. Prasad, R.S. Ningthoujam, S.J. Ghosh, S.H. Pawar, Magnetic chitosan nanocomposite for hyperthermia therapy application: preparation, characterization and in vitro experiments, Appl. Surf. Sci. 288 (2014) 149-157.

[42] Q. Yang, Y. Zhu, M. Yang, S. Ma, Y. Wu, F. Lan, Z. Gu, Ligand-free Fe_3O_4/CMCS nanoclusters with negative charges for efficient structure-selective protein adsorption, Small 12 (17) (2016) 2344-2353.

[43] A. Zhu, L. Yuan, T. Liao, Suspension of Fe_3O_4 nanoparticles stabilized by chitosan and o-carbo-xymethylchitosan, Int. J. Pharm. 350 (1-2) (2008) 361-368.

[44] N.D. Cuong, T.T. Hoa, D.Q. Khieu, T.D. Lam, N.D. Hoa, N.V. Hieu, Synthesis, characterization, and comparative gas-sensing properties of Fe_2O_3 prepared from Fe_3O_4 and Fe_3O_4-chitosan, J. Alloys Compd. 523 (2012) 120-126.

[45] V. Belessi, R. Zboril, J. Tucek, Ferrofluids from magnetic-chitosan hybrids, Chem. Mater. 20 (10) (2008) 3298-3305.

[46] C.-H. Kuo, Y.-C. Liu, C.-M.J. Chang, J.-H. Chen, C. Chang, C.-J. Shieh, Optimum conditions for lipase immobilization on chitosan-coated Fe_3O_4 nanoparticles, Carbohydr. Polym. 87 (4) (2012) 2538-2545.

[47] A. Lopez-Cruz, C. Barrera, V.L. Caledo-DdelC, C. Rinadi, Water dispersible iron oxide nanoparticles coated with covalently linked chitosan, J. Mater. Chem. 19 (37) (2009) 6870-6876.

[48] A. Mohseni-Bandpi, B. Kakavandi, R.R. Kalantary, A. Azari, A. Keramati, Development of a novel magnetite–chitosan composite for the removal of fluoride from drinking water: adsorption modeling and optimization, RSC Adv. 5 (89) (2015) 73279-73289.

[49] J. Mohapatra, A. Mitra, D. Bahadur, M. Aslam, Surface controlled synthesis of MFe_2O_4 (M = Mn, Fe, Co, Ni and Zn) nanoparticles and their magnetic characteristics, CrystEngComm. 15 (3) (2013) 524-532.

Figure captions:

Fig. 1. XRD pattern (a) and TEM image (b) of lumpy-shaped magnetite-chitosan nanostructures.

Fig. 2. Schematic representation of the formation of magnetite-chitosan composites.

Fig. 3. XRD pattern (a) and TEM image (b) of spherical nanostructures.

Fig. 4. EDS mapping of rice-seed-like nanostructures.

Fig. 5. TEM image of rice-seed-like nanostructures.

Fig. 6. TEM image of chitosan coated magnetite-chitosan nanostructures.

Fig. 7. EDS mapping of chitosan coated nanostructures.

Fig. 8. Hysteresis loops of (a) rice-seed-like and (b) chitosan coated spherical nanostructures. The insets show the low field part of the loops.

Table 1. Synthesis parameters and morphology of magnetite-chitosan nanostructures

Synthesis parameters	Shape	Size (nm)	Characterization technique	Fig.
0.01 M Fe^{2+}, 0.02 M Fe^{3+}, 80 ^{o}C, 50 h[a]	Lumpy	75–150	XRD, TEM	1
0.05 M Fe^{2+}, 0.1 M Fe^{3+}, 80 ^{o}C, 10 h[a]	Spherical	9–18		3
0.05 M Fe^{2+}, 0.1 M Fe^{3+}, 80 ^{o}C, 50 h[a]	Rice-seed-like, quasi-spherical	75–290	TEM/EDS, SQUID	4, 8a
0.08 M Fe^{2+}, 0.16 M Fe^{3+}, 80 ^{o}C, 50 h[a]			TEM	5
0.05 M Fe^{2+}, 0.1 M Fe^{3+}, 80 ^{o}C, 50 h, chitosan:iron chlorides = 3:1	Spherical with chitosan coating	35–120	TEM/EDS, SQUID	6, 7, 8b

[a] The weight ratio of chitosan to iron chlorides was 1:1.

Table 2. Synthesis conditions, morphology, and magnetic properties of magnetite-chitosan composites at room temperature

Method	Temperature/time	Shape	Size (nm)	*Hc* (Oe)	*Ms* (emu/g)	Ref.
Precipitation[a]	80 °C/50 h	Rice-seed-like, quasi-spherical	75–290	140	56.7	this study
			35–120	80	27.2	
Precipitation[b]	70 °C/1 h		0.6-13 μm	311	22	[32]
Precipitation[a]	-		25–30	-	55	[33]
Spray-precipitation[b]	60 °C/-		10.3	58.4	25.6	[34]
Oxidation-precipitation[b]	70 °C/30 min; 40 °C/2 h		160	-	37.2	[35]
Precipitation[a]	50 °C/50 min	Spherical	9.9–11	27.09	66.35	[36]
Hydrothermal[a]	200 °C/8 h		100–150	-	30.8	[37]
Hydrothermal[a]	185 °C/48 h		200	-	39.5	[38]
Reverse microemulsion precipitation[a]	70-80 °C/30 min		3–6	6.1	52.9	[39]
Sonochemical[b]	-/1 h		11–18	24.06	38.57	[40]
Precipitation[b]	60 °C/-		10–20	13.29	49.96	[41]
Precipitation[b]	80 °C/1 h		~500	-	60	[42]
Precipitation[b]	-	Spherical, ellipsoidal	13–20	4.5	39.1	[43]
Precipitation[b]	80 °C/30 min		10–20	-	60	[44]
Precipitation[b]	60 °C/1 h	Cubic	20–40	-	63	[45]

Precipitation[b]	80 °C/30 min	Quasi-spherical	30	-	60	[46]
Thermolysis[b]	320 °C/30 min	Spherical, cubic	40–80	-	60	[47]
Precipitation[a]	100 °C/1 h	Spherical, polyhedral	20–50	-	34.5	[48]

[a] Synthesis in the presence of chitosan.

[b] Synthesis of Fe_3O_4 nanoparticles was followed by chitosan coating procedure.

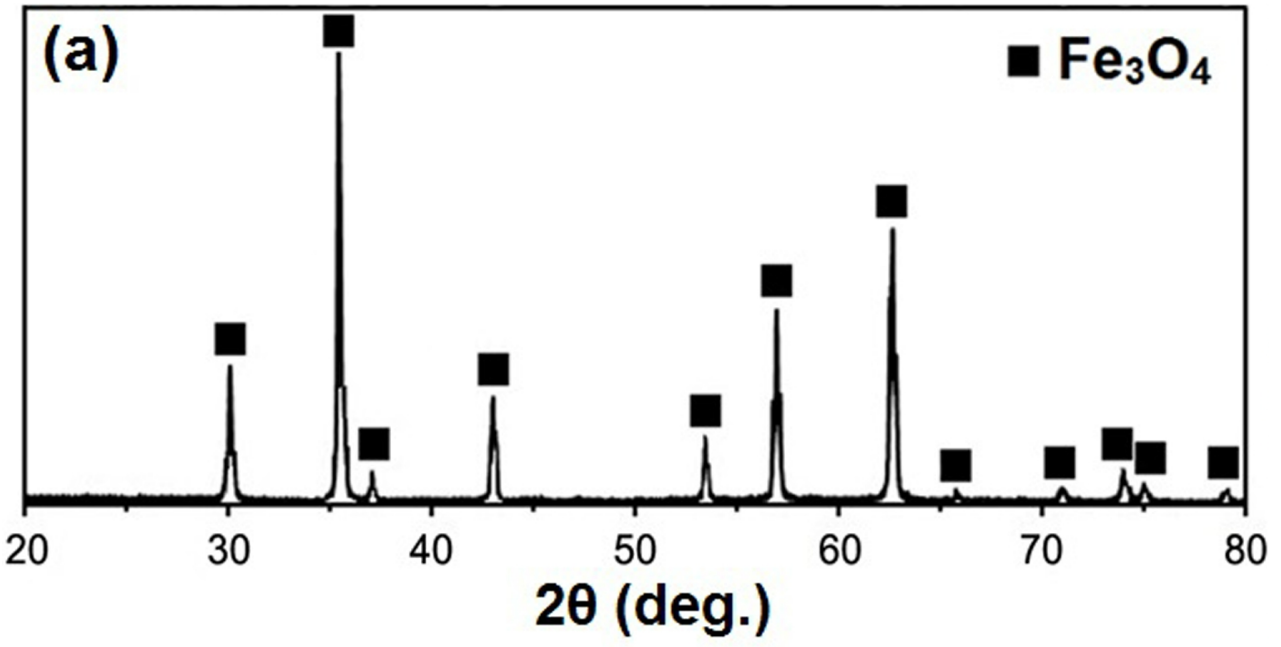
(a)
■ Fe3O4
20
30
40
50
60
70
80
2θ (deg.)

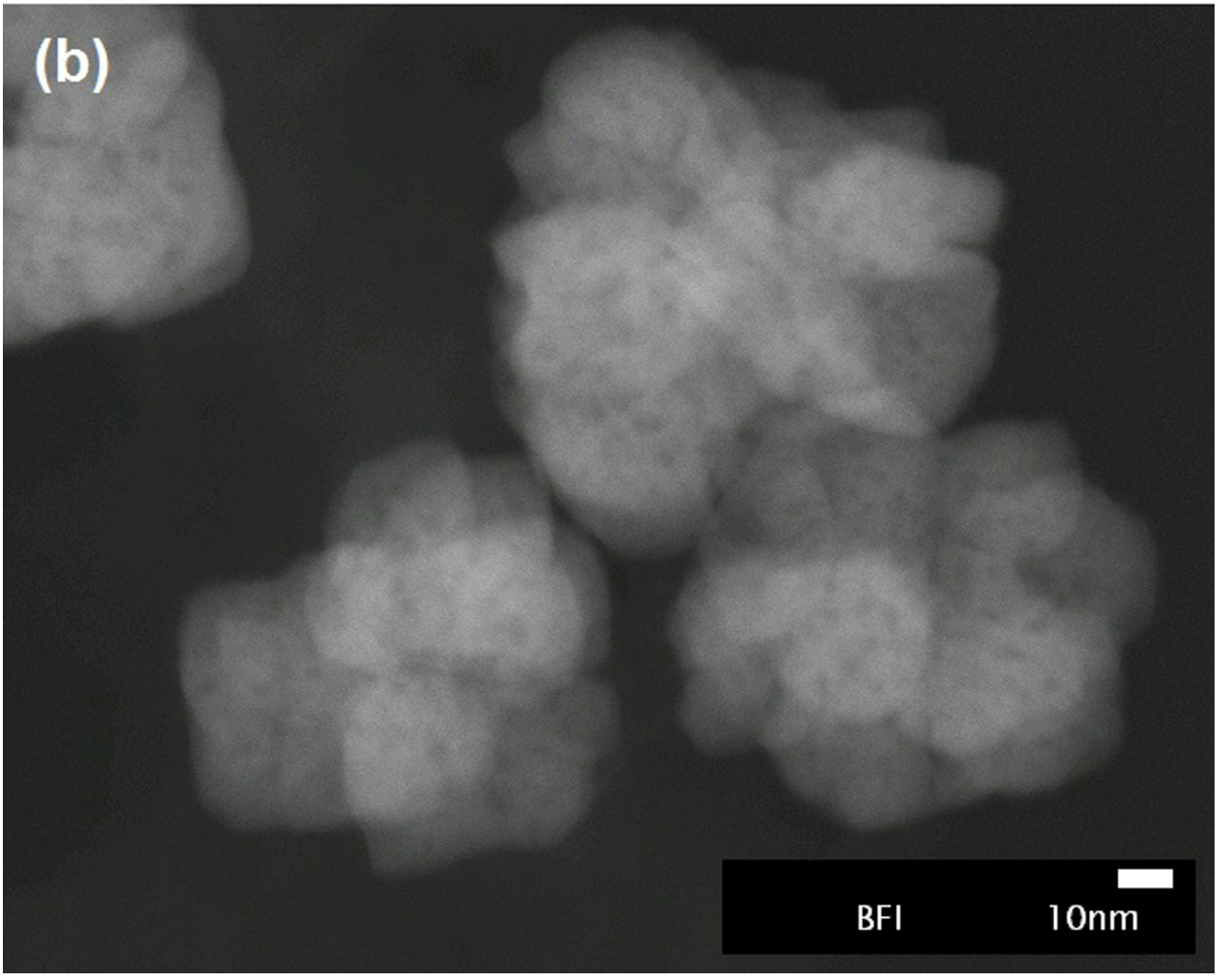
(b)
BFI
10nm

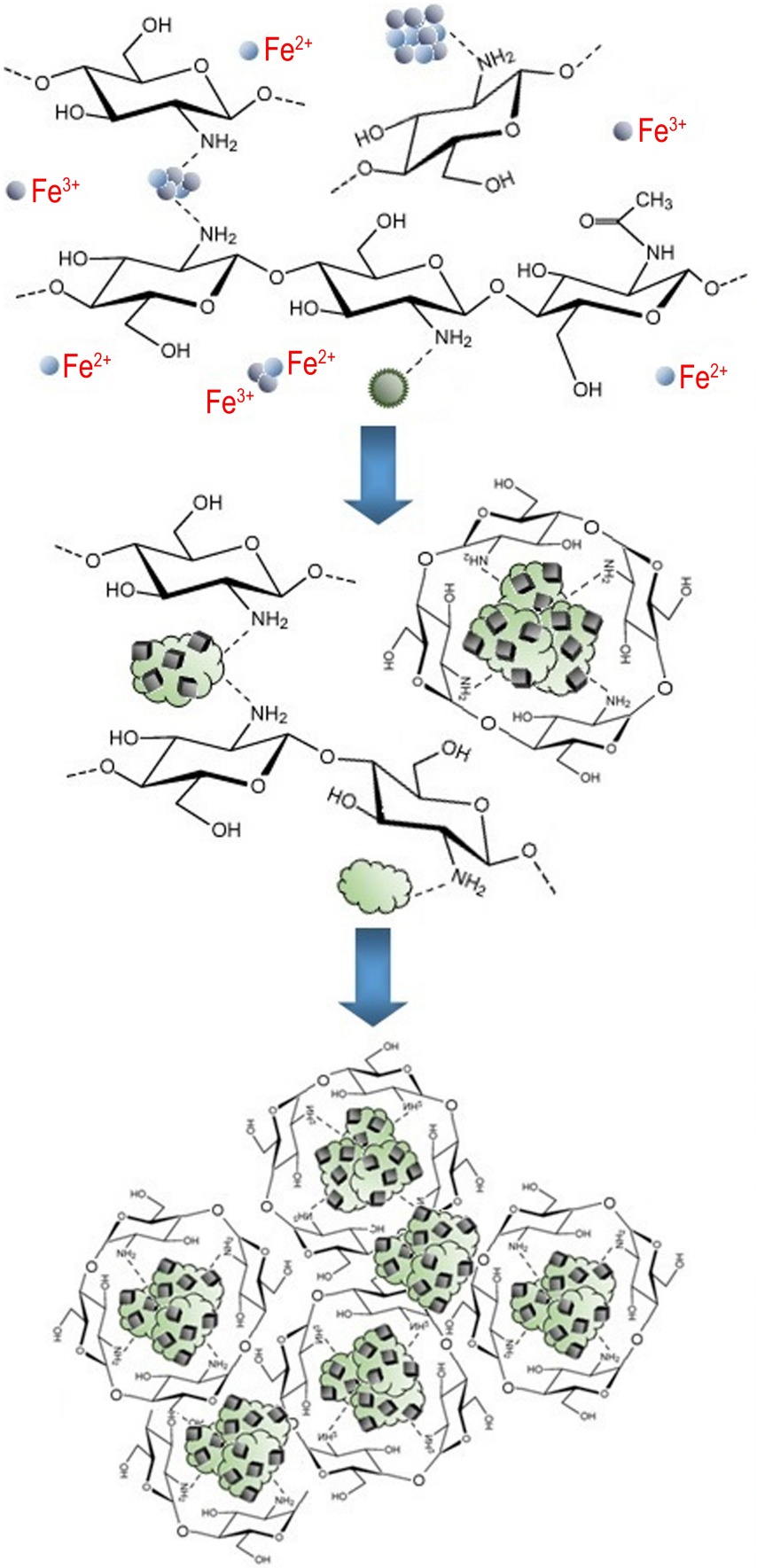
Fe2+
Fe3+
– iron ions
– aggregated Fe3O4 nuclei
– Fe3O4 nuclei
– Fe3O4 nanocrystals

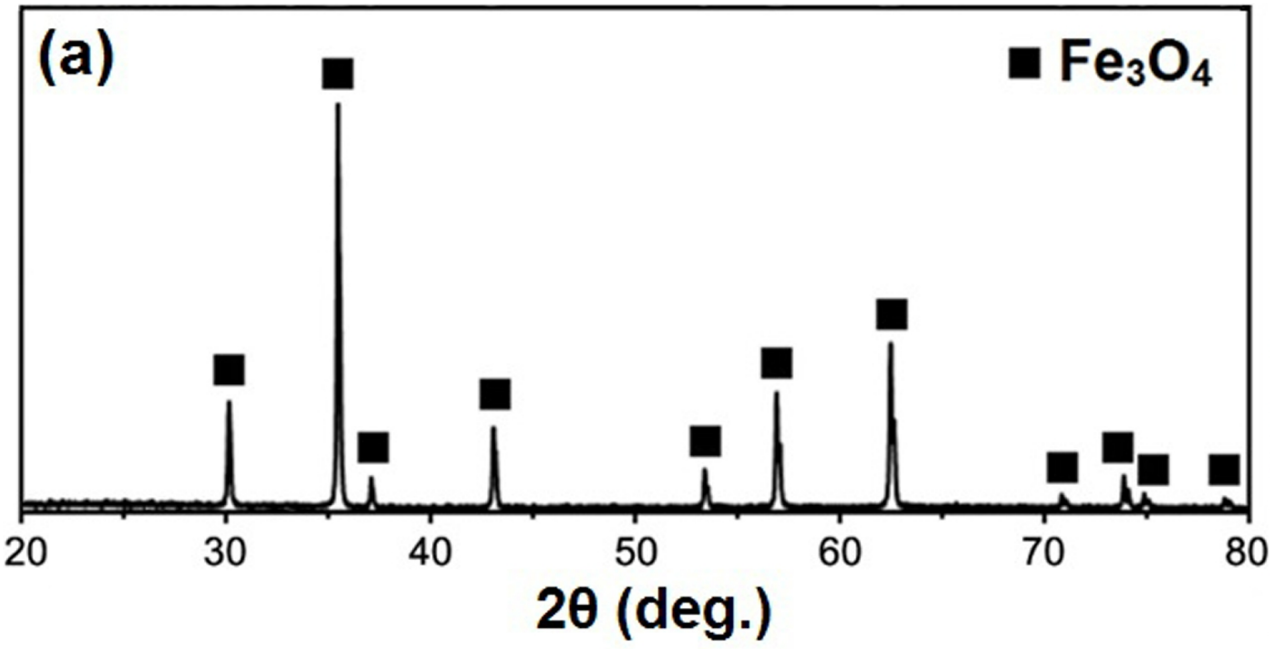
(a)
■ Fe3O4
20
30
40
50
60
70
80
2θ (deg.)

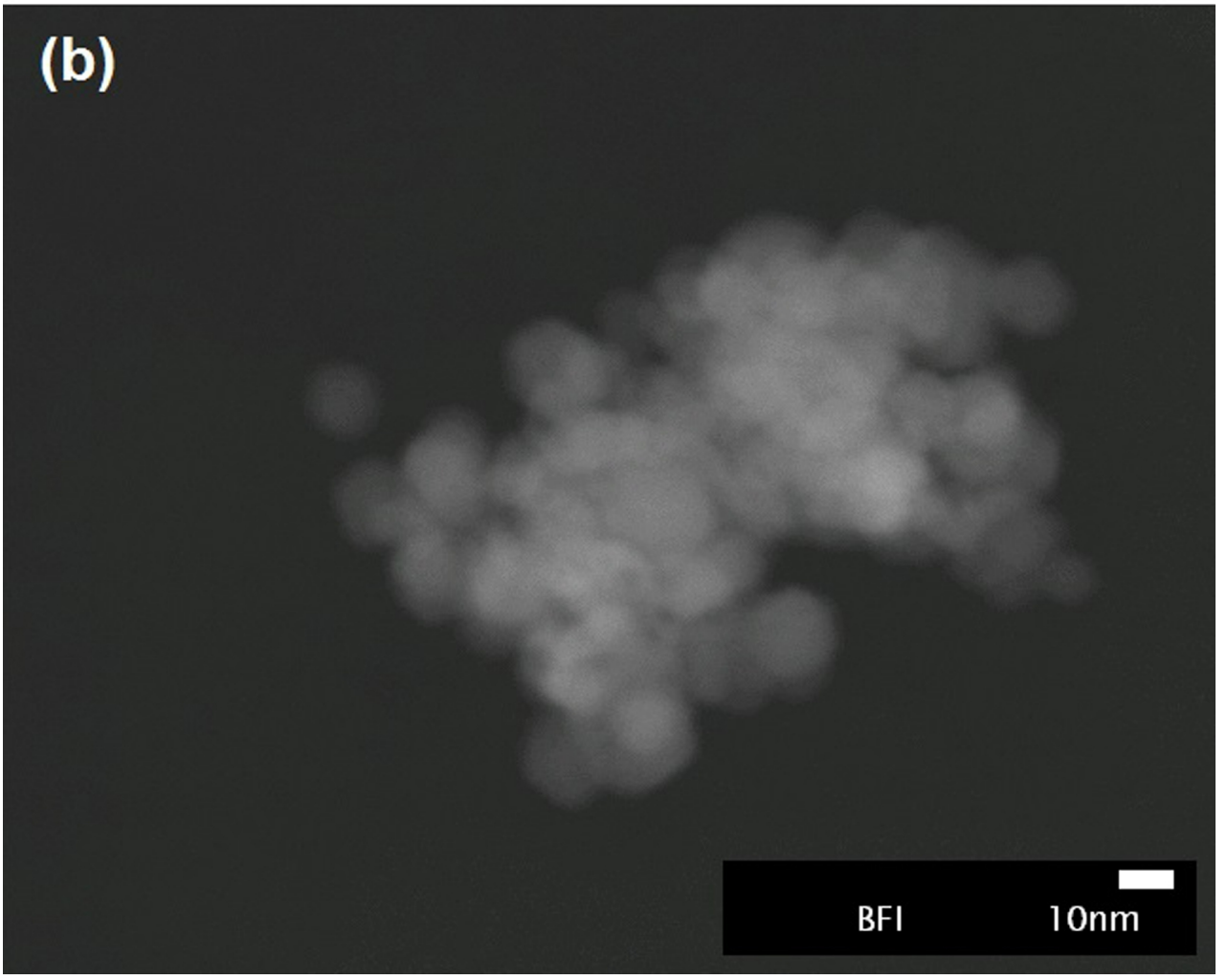
(b)
BFI
10nm

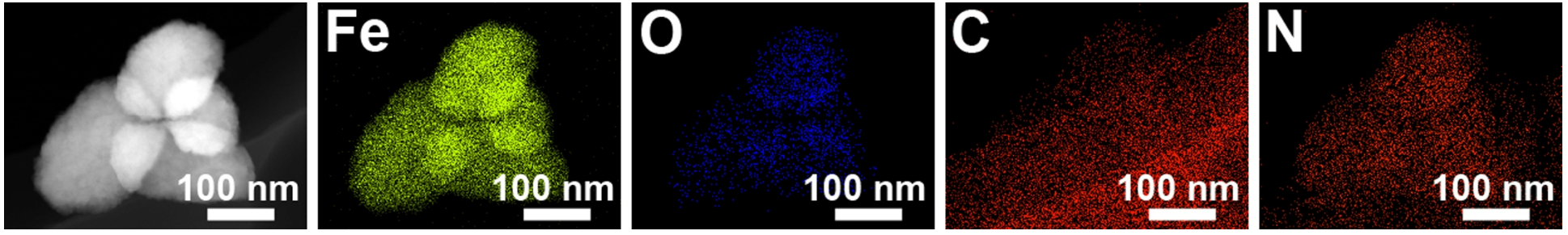
100 nm
Fe
100 nm
O
100 nm
C
100 nm
N
100 nm

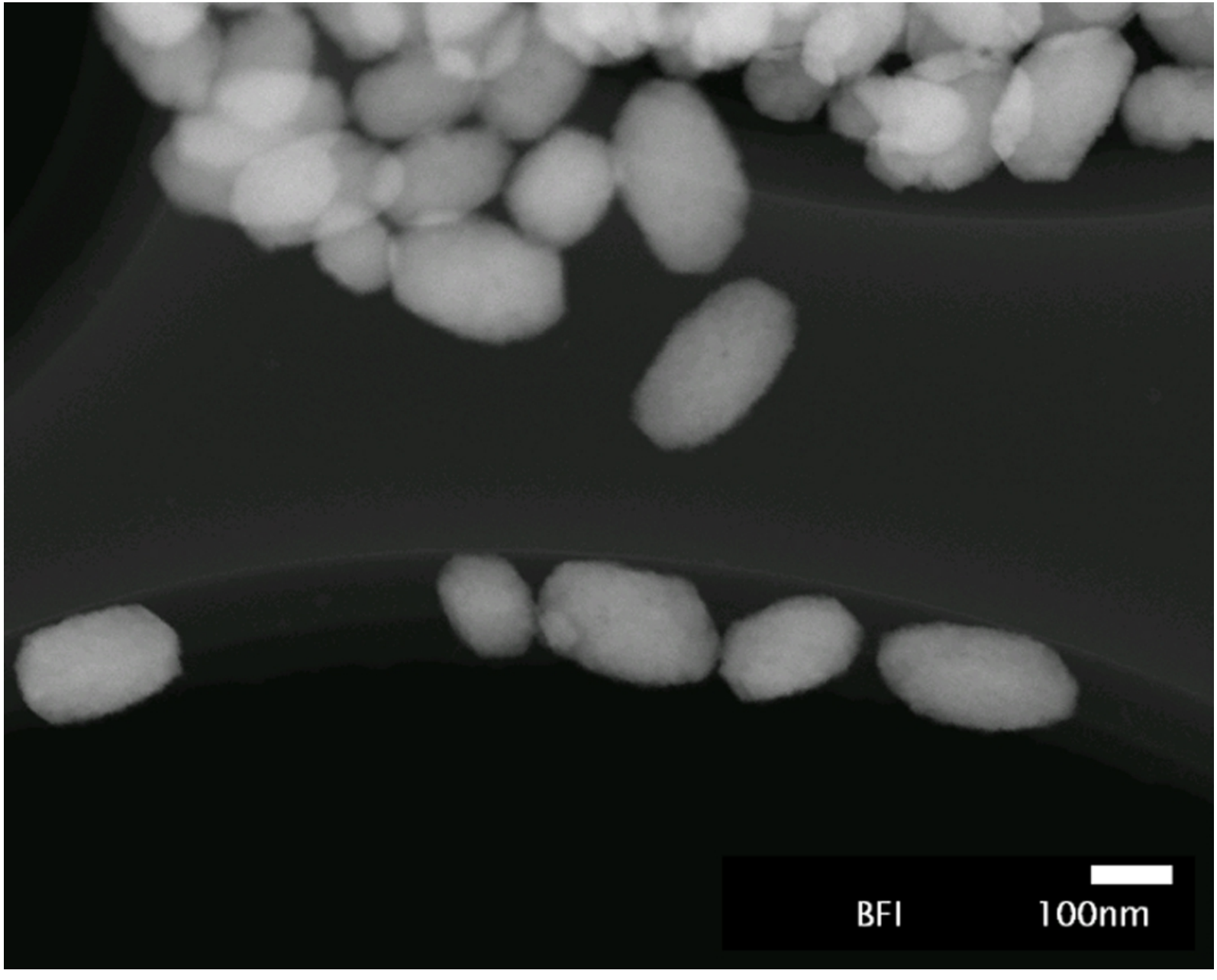
BFI
100nm

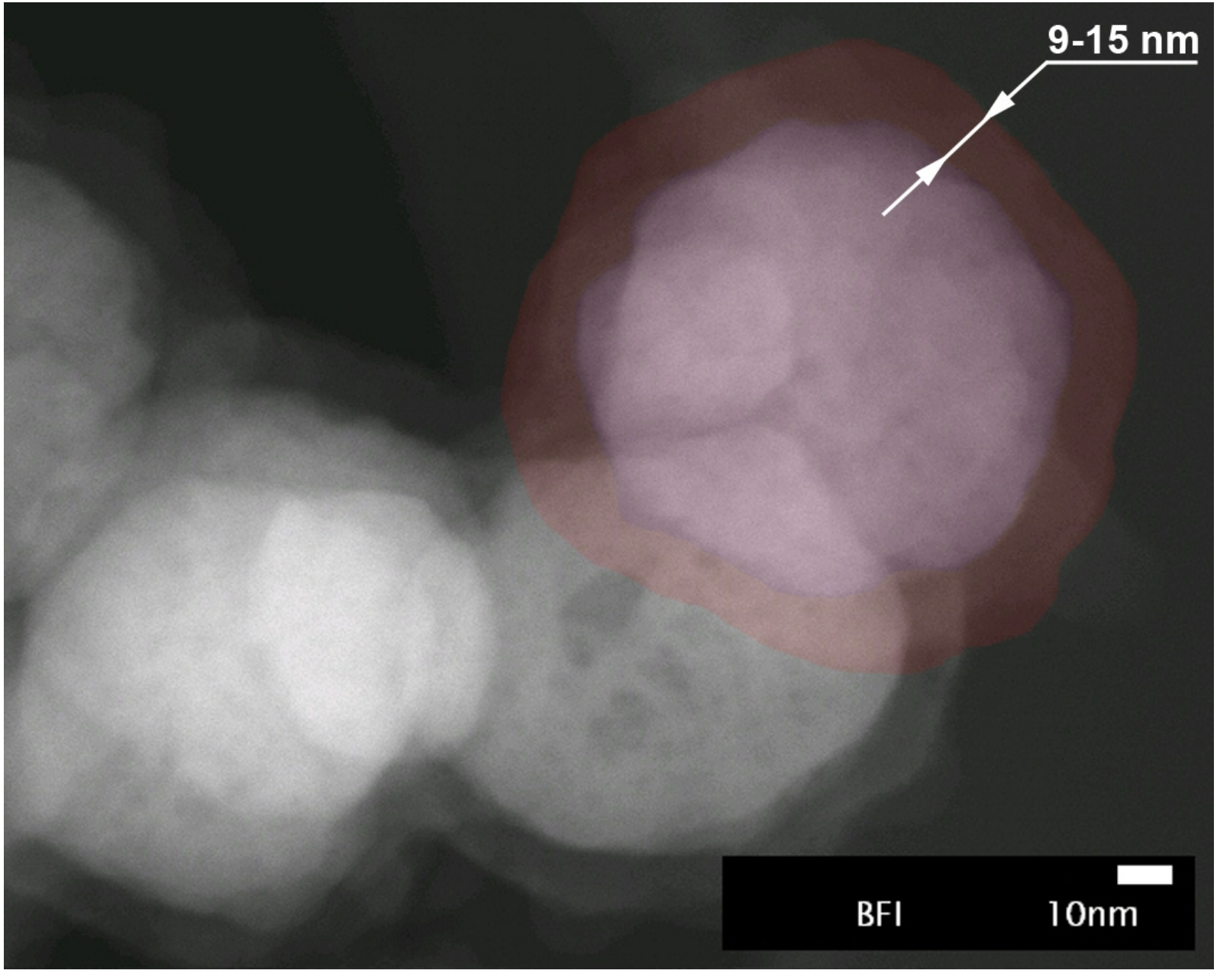
9-15 nm
BFI
10nm

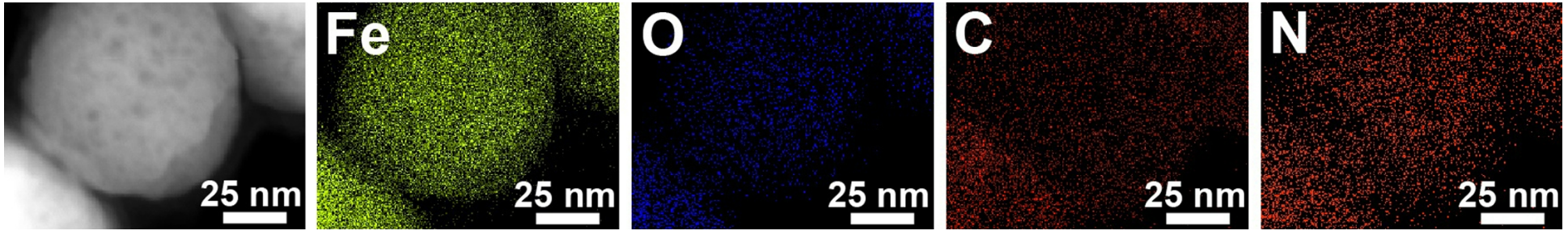
25 nm
Fe
25 nm
O
25 nm
C
25 nm
N
25 nm

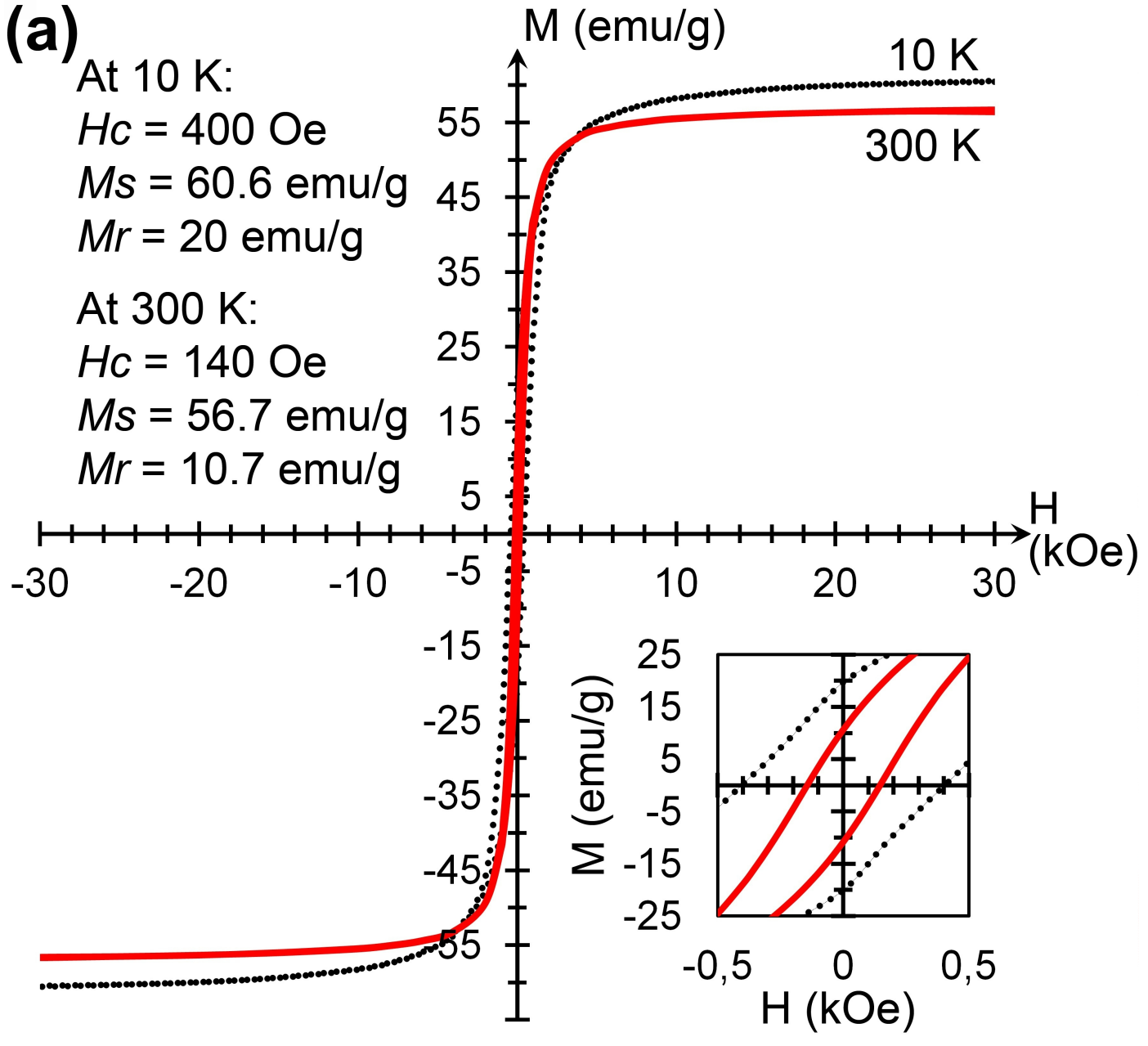
(a)
At 10 K:
Hc = 400 Oe
Ms = 60.6 emu/g
Mr = 20 emu/g
At 300 K:
Hc = 140 Oe
Ms = 56.7 emu/g
Mr = 10.7 emu/g
M (emu/g)
10 K
300 K
55
45
35
25
15
5
-5
-15
-25
-35
-45
-55
H
(kOe)
-30
-20
-10
10
20
30
M (emu/g)
25
15
5
-5
-15
-25
-0,5
0
0,5
H (kOe)

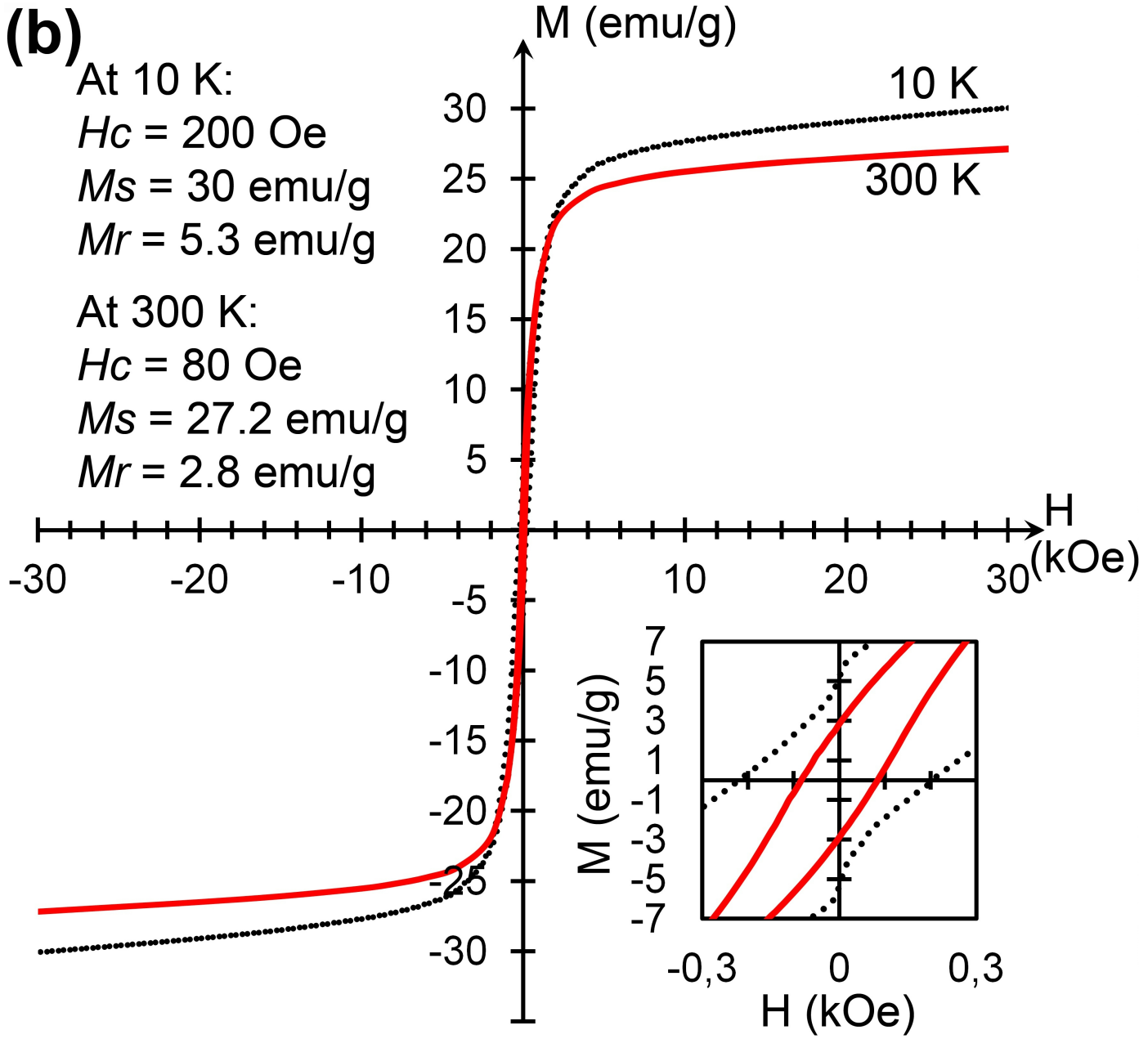
(b)
At 10 K:
Hc = 200 Oe
Ms = 30 emu/g
Mr = 5.3 emu/g
At 300 K:
Hc = 80 Oe
Ms = 27.2 emu/g
Mr = 2.8 emu/g
M (emu/g)
10 K
300 K
H (kOe)
30
25
20
15
10
5
-5
-10
-15
-20
-25
-30
-30
-20
-10
10
20
30
M (emu/g)
7
5
3
1
-1
-3
-5
-7
-0,3
0
0,3
H (kOe)

Highlights

- Magnetite-chitosan nanostructures are synthesized via self-assembly.
- Different morphology can be obtained by adjusting the synthesis parameters.
- An attractive combination of magnetic properties and morphology is obtained.
- Magnetite-chitosan nanostructures are ferrimagnetic and pseudo-single domain.